Droop Control with Improved Disturbance Adaption for PV System with Two Power Conversion Stages

Liu, Hongpeng; Loh, Poh Chiang; Wang, Xiongfei; Yang, Yongheng; Wang, Wei; Xu, Dianguo

Published in:
I E E E Transactions on Industrial Electronics

DOI (link to publication from Publisher):
10.1109/TIE.2016.2580525

Publication date:
2016

Document Version
Accepted author manuscript, peer reviewed version

Droop Control with Improved Disturbance Adaption for PV System with Two Power Conversion Stages

Hongpeng Liu, *Member, IEEE*, Poh Chiang Loh, Xiongfei Wang, *Member, IEEE*, Yongheng Yang, *Member, IEEE*, Wei Wang, *Member, IEEE,* and Dianguo Xu, *Senior Member, IEEE*

***Abstract*—Droop control has commonly been used with distributed generators for relating their terminal parameters with power generation. The generators have also been assumed to have enough capacities for supplying the required power. This is however not always true, especially with renewable sources with no or insufficient storage for cushioning climatic changes. In addition, most droop-controlled literatures have assumed a single dc-ac inverter with its input dc source fixed. Front-end dc-dc converter added to a two-stage photovoltaic (PV) system has therefore usually been ignored. To address these unresolved issues, an improved droop scheme for a two-stage PV system has been developed in the paper. The developed scheme uses the same control structure in both grid-connected and islanded modes, which together with properly tuned synchronizers, allows mode transfer to be seamlessly triggered. Moreover, the proposed scheme adapts well with internal PV and external grid fluctuations, and is hence more precise with its tracking, as compared with the traditional droop scheme. Simulation and experimental results have verified these expectations, and hence the effectiveness of the proposed scheme.**

***Index Terms*—Microgrid, PV system, droop control, islanded mode, grid-connected mode, seamless transfer.**

I. Introduction

Formation of microgrid (MG) is an attractive approach for solving energy challenges experienced around the globe [1], [2]. It has thus been widely studied in either its grid-connected or islanded mode [3]-[5]. In the former, interfacing inverters are normally operated as controlled current sources, injecting active and reactive powers to the grid [6]. Alternatively, they can be voltage-controlled like proposed in [7]-[20]. For example, in [7], a single-phase PV system has been voltage-controlled to support the fundamental voltage, while eliminate harmonics at its point of common coupling (PCC). The approach however adds an extra inductor in series with the grid to make it more inductive at the expense of size and efficiency.

Another well-received approach is indirect current control, where the grid current has been controlled by regulating magnitude and phase of the ac filter capacitor voltage [8], [9]. Its design is however complex because of nonlinear factors, and sine and cosine tables included in the control. A simplification has subsequently been developed in [10] without the sine and cosine tables. The controller can then be designed using classical control techniques. Despite that, the load voltage waveform may still be distorted since it is not regulated directly by a voltage control loop. A further improvement can be found in [11], where the control system has been enhanced by connecting a local load to the filter capacitor, before feeding back the capacitor current for control. The method works fine, but its dc-link dynamic has not been addressed.

The next voltage-controlled technique proposed is the droop method, which in effect, has mapped the generator terminal parameters with its active and reactive power generations [12]-[14]. The droop method is originally borrowed from large synchronous generators connected to the power grids [15], but when applied to smaller distributed generators (DGs), is prone to fluctuations because of the absence of large inertias and fuel reserves. Despite that, the droop concept has been commonly used with [16] and [17] presenting a droop controller for DG that can guarantee zero steady-state error for its output reactive power. Its output active power may however deviate from the desired reference value. To solve the problem, integral terms have been added to the conventional droop scheme for forcing the DG active and reactive powers to track their references closely [18].

The droop principle has also been recommended by the Consortium for Electric Reliability Technology Solutions (CERTS) for regulating photovoltaic (PV) inverters with a stable bus voltage, even during load transient [19]. More recently, a universal controller has been proposed in [20], where maximum-power-point-tracking (MPPT), droop control

Manuscript received September 16, 2015; revised February 13, 2016 and April 06, 2016; accepted May 04, 2016. This work was supported by the National Natural Science Foundation of China under Grant 51477033, and in part by the Lite-On Power Electronics Technology Research Fund under Grant PRC20151382.

H. Liu, W. Wang, and D. Xu are with the Department of Electrical Engineering, Harbin Institute of Technology, Harbin 150001, China (e-mail: lhp602@hit.edu.cn; wangwei602@hit.edu.cn; xudiang@hit.edu.cn).

P. C. Loh, X. Wang, and Y. Yang are with the Department of Energy Technology, Aalborg University, Aalborg DK-9220, Denmark (e-mail: pcl@et.aau.dk; xwa@et.aau.dk; yoy@et.aau.dk).

and dc-link voltage regulation have been managed simultaneously without major control reconfiguration. The limitation introduced is other non-renewable sources or storage units must be present for balancing supply and demand, which if not catered, will severely narrow variation range of the loads. Despite these differences, the studies in [16] to [20] have not considered possible fluctuations of the dc source connected to the inverter. Such consideration is relevant to renewable sources like PV, where variations may be unintentionally caused by changes of irradiation or intentionally activated by the MPPT scheme. In addition, the studies have only focused on single-stage converters, which make them not directly applicable to two-stage converters used with some PV systems.

The other concern investigated is the uninterrupted supply of power, which will then require seamless transfer between grid-connected and islanded modes [21]-[28]. For example, [23] has proposed a high-performance inverter controlled by an adaptive sliding-mode scheme. Sliding-mode control is generally fast, and can hence ride through the transfer smoothly. However, it is nonlinear and mathematically complex, which may make analysis difficult. In [24], a voltage-current-weighted control has been proposed with different weights used for its grid-connected and islanded modes during the transfer. It uses four controllers in total, and is hence equally complex. In [25] and [26], the transfer is accompanied by a reconfiguration of controllers, which supposedly, is a non-optimized solution when compared with schemes that use a single common control structure throughout the transfer. Such common control schemes are however not widely discussed at present.

Moreover, seamless transfer requires synchronization with the grid, prior to connecting an islanded DG with the mains [29], [30]. For single-phase inverters, zero-crossing detection of the grid voltage is a possible technique, but sensitive to grid voltage distortion [31]. Another synchronization technique has therefore been presented in [32] for P–f and Q–V droop-controlled DG. The technique uses one synchronizer for eliminating voltage magnitude difference and another for eliminating phase difference between the DG and grid. It is however formulated for an inductive grid only, and not the predominantly resistive low-voltage (LV) distribution network. Similar synchronization concepts can however still be used, but only after some minor modifications are added to account for its resistive characteristics.

Summarizing the above, presently unresolved issues are listed, as follows.

- Studies, including [12] to [19], have considered single-stage inverters with sufficient generation capacities. This may not be true for PV systems, where two-stage converters with no or limited storage may sometimes be used.
- Effects of internal and external fluctuations on the droop performances have usually been neglected. This may not be appropriate for PV systems, where climatic changes are common.
- A common droop structure with the first two issues resolved has not been developed for ensuring seamless transfer between operating modes.

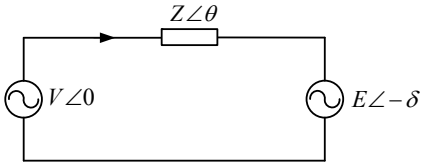

Fig. 1. Simplified circuit for illustrating power transfer.

These challenges have been addressed in the paper by proposing an improved droop scheme for two-stage PV systems. Simulation and experimental results have verified the expected performances of the proposed scheme.

II. General Power Transfer and Possible Variations

Fig. 1 shows a simple circuit for formulating power transfer. The notations used are $V\angle 0$, $Z\angle\theta$ and $E\angle$-δ (V and E are peak values) for representing output voltage from the PV system, line impedance and voltage at the PCC, respectively. In the grid-connected mode, $E\angle$-δ is decided by the grid, while in the islanded mode, it is determined by the local generators and loads. Regardless of that, power angle δ is usually small, which means $\sin\delta \approx \delta$ and $\cos\delta \approx 1$ can be used for simplification. In addition, for a LV distribution network, the line impedance is mainly resistive, which means $\theta \approx 0$. The active and reactive powers (P and Q) transferred can thus be expressed as:

$$P = \frac{V(V-E)}{Z} \tag{1}$$

$$Q = -\frac{VE}{Z}\delta. \tag{2}$$

These equations show that active power can be controlled by adjusting V, while reactive power can be controlled by varying δ, even though it is also affected by V. Additionally, both powers are affected by disturbances from E and Z, which strictly, are external of the PV system. Internally within the PV system, active power limitation can also happen because of a drop in irradiation, for example. Specific details related to these issues are discussed separately in the next two sections for the islanded and grid-connected modes.

III. Islanded Mode

A. Control Principle

Beginning with active power transfer represented by (1), a P-V curve can be plotted, as shown in Fig. 2(a). This curve will shift when E and / or Z vary, as understood from (1). Regardless of that, the P-V curve alone is not sufficient for defining a specific operating point for the network. To mark out this stable operating point, the PV system must be controlled to add a second P-V curve to Fig. 2(a), which conventionally, has assumed the linear droop characteristic represented by (3) [33].

$$V = V_0 - k_p(P - P_0) \tag{3}$$

$$f = f_0 + k_q(Q - Q_0) \tag{4}$$

where f and f_0 are the measured and rated frequencies of the PV system, V and V_0 are the measured and rated output voltage

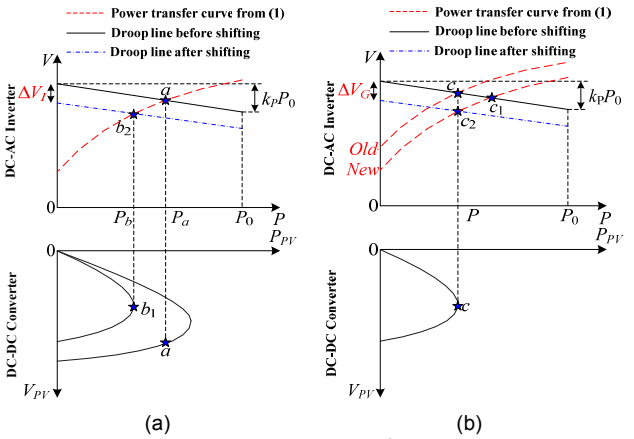

Fig. 2. *P-V* interactions during changes of (a) PV power and (b) grid voltage.

amplitudes, P_0 and Q_0 are the rated active and reactive powers, and k_p and k_q are the active and reactive droop coefficients, respectively. An intersection at point a is thus created, whose corresponding operating point on the PV curve is also marked with the same notation of a. In the steady state, both operating points must have the same power value P_a, in order to keep the dc-link voltage stabilized.

The same reasoning can be applied to reactive power transfer, which then necessitates the Q-f droop expression in (4) for controlling the PV system. It is however not possible to draw (2) and (4) on a single diagram because of their differences in one of the parameters (δ and f, where $\delta = 2\pi ft + \delta_0$, and δ_0 is the initial power angle). Implementation of (3) and (4) then results in a control scheme similar to that shown in Fig. 3 for a two-stage PV system when in its islanded mode. The only difference is Fig. 3 includes a modified active power droop expression, instead of (3). The modified droop expression will be explained later. Regardless of that, Fig. 3 shows the output voltage v_{ac} and current i_{ac} of the rear-end inverter being measured for computing P and Q. The active and reactive droop expressions can then be used for mapping out the desired V and f, from which the demanded voltage reference v_{ref} is computed for tracking by the usual double-loop controller. On the other hand, the front-end boost converter is controlled by a single-loop voltage converter notated as $G_B(s)$. Input to $G_B(s)$ is the difference between the measured dc-link voltage V_{DC} and its reference V_{DCref}. To nullify this difference, $G_B(s)$ is usually a proportional-integral (PI) controller, which may not be necessary for the proposed scheme because of reasons explained next.

As described earlier, the P-V curve and line in Fig. 2(a) help to define a common operating point with $P = P_a$. In the literature, this active power has always been assumed as supplied by the DG without difficulty [14], [34]. Such assumption is however true only when a large reserve of fuel or storage is available for cushioning variations of parameters, which for a PV system, are its irradiation and temperature. Assuming now that the reserve is not catered and the PV maximum power P_{PVmax} has been reduced such that $P_{PVmax} < P_a$ in Fig. 2(a) (see point b_1), power delivered to the dc-link by the

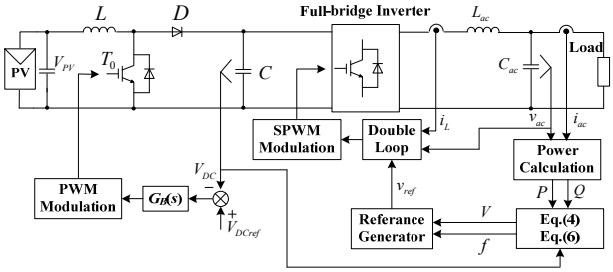

Fig. 3. Control scheme for two-stage PV system in islanded mode (transformer used in practice and experiment not shown for conciseness).

boost converter will then be lesser than power drawn out from it by the inverter. The dc-link voltage will therefore drop until the inverter power is reduced to $P = P_b = P_{PVmax}$, which in Fig. 2(a), is achieved by lowering the droop line by ΔV_I (see point b_2).

The challenge is finding the value for ΔV_I, which the simplest method is to compute it using a PI controller. Input to the PI controller can be the difference between power delivered by the dc-dc converter to the dc-link capacitor and power extracted from the same capacitor by the inverter. However, in the steady state, this power imbalance will reduce to zero (ignoring losses) before the dc-link capacitor voltage can stabilize. Despite that, the integral term of the PI controller will still output a finite ΔV_I for lowering the droop line in Fig. 2(a). Value of the PI controller output is however not specific, because of its single-to-multiple mapping characteristic, which is usually not encouraged when multiple converters are connected in parallel. Because of that, the proportional droop scheme without any integral term is used instead for finding ΔV_I.

Instead, the dc-link voltage V_{DC} is allowed to vary within a very small range, notated as $V_{DCmin} \le V_{DC} \le V_{DCref}$. The lower limit of the range must at least be higher than the maximum inverter output voltage to avoid over-modulation. The necessary expression governing it can thus be derived from (3) as $V_{DCmin} \ge V_0 + k_p P_0$, after substituting $P = 0$. The required ΔV_I can then be computed from (5), based on the same proportional droop principle.

$$\Delta V_I = \begin{cases} k_V \left(V_{DC} - V_{DCref} \right), & V_{DC} < V_{DCref} \\ 0, & V_{DC} \ge V_{DCref} \end{cases} \qquad (5)$$
$$-k_p P_0 \le \Delta V_I \le 0$$

where k_V is the droop coefficient for computing ΔV_I.

Some insights drawn from (5) are summarized, as follows.

- Offset ΔV_I varies in the range of $-k_p P_0 \le \Delta V_I \le 0$. Lower limit $-k_p P_0$ is obtained by subtracting the maximum of (3) from its minimum ($V_0 - (V_0 + k_p P_0)$).
- The actual V_{DC}, when fallen below V_{DCref}, represents a lack of PV capacity (e.g. insufficient irradiation) for restoring the dc-link voltage. The inverter power must hence be lowered by introducing a negative ΔV_I.
- The actual V_{DC}, when risen above V_{DCref}, represents an excess PV capacity (e.g. strong irradiation), which can be lowered to meet the lower load demand. No offset ($\Delta V_I = 0$) is thus added for changing the inverter power.
- As V_{DC} is now required to vary, controller $G_B(s)$ for the

boost converter cannot be a PI controller. It should be a proportional droop controller with gain given by ($V_{DCref} - V_{DCmin}$) / P_0.

- Coefficient k_V will usually be high if only a narrow dc-link voltage range is permitted (partly due to the large dc-link capacitor C included for decoupling purposes).

The modified P-V droop expression is then written as (6), where the first term is the usual droop expression for power sharing, and the second term is for regulating internal power limitation within the generator.

$$V = \underbrace{V_0 - k_p(P - P_0)} + \underbrace{k_V(V_{DC} - V_{DCref})} \tag{6}$$

The Q-f expression, on the other hand, remains unchanged, since internal active power variation will not limit the amount of reactive power that the rear-end inverter can deliver. This explains why the reactive power droop expression in Fig. 3 has been retained as (4), while the active power droop expression has been changed to (6). Moreover, it should be emphasized that Fig. 3 works even with a limited amount of storage (mainly for catering much lower night usage) added to the dc-link of each PV system through a second dc-dc converter. This storage can charge when its charger detects V_{DC} above V_{DCref}, which as aforementioned represents an excess PV capacity. On the other hand, it may discharge when V_{DC} falls below V_{DCref} to reinforce the lack of PV capacity, if necessary. The dc-link voltage will then stabilize, but if the interval of insufficient PV capacity is longer than that the storage capacity can support, the dc-link voltage will eventually continue its drop, allowing (6) to work as intended. The control scheme in Fig. 3 with (6) included can thus be used without changes, even with some storage introduced through a second dc-dc converter at the dc-link.

B. Small-Signal Analysis

Small-signal analysis can next be performed on (4) and (6) for studying the behaviors of paralleled converters, whose number has been kept at two to avoid excessive mathematical complexity. Output voltages of these two converters can further be notated as $\dot{V}_1 = V_{d1} + jV_{q1}$ and $\dot{V}_2 = V_{d2} + jV_{q2}$, respectively. Their angles and magnitudes can then be expressed as:

$$\delta_i = \arctan\left(\frac{V_{qi}}{V_{di}}\right) \tag{7}$$

$$V_i = \left|V_{di} + jV_{qi}\right| = \sqrt{V_{di}^2 + V_{qi}^2} \tag{8}$$

where i = 1 or 2 is the assigned converter index number.

The variation of energy E_i in each dc-link capacitor of the converter can also be written as:

$$E_i = \int P_i(t)dt = \frac{1}{2}CV_{DCref}^2 - \frac{1}{2}CV_{DCi}^2 \tag{9}$$

where V_{DCi} and C are the dc-link voltage and capacitance, respectively. The linearly perturbed expression for relating the dc-link voltage and its power can thus be derived as:

$$\Delta V_{DCi} = -\frac{1}{mCs}\cdot\Delta P_i = -\frac{k_{DC}}{s}\cdot\Delta P_i \tag{10}$$

where m is the equilibrium value of V_{DCi}, and Δ is for representing perturbation. Additionally, $\Delta f_i = s\Delta\delta_i/2\pi$. Combining these perturbed expressions with the small-signal expressions of (4) and (6) then results in the state equation (11) for representing each converter.

$$\begin{bmatrix}\Delta\dot{V}_{DCi}\\ \Delta\dot{f}_i\\ \Delta\dot{V}_{di}\\ \Delta\dot{V}_{qi}\end{bmatrix} = A_i\begin{bmatrix}\Delta V_{DCi}\\ \Delta f_i\\ \Delta V_{di}\\ \Delta V_{qi}\end{bmatrix} + B_i\begin{bmatrix}\Delta P_i\\ \Delta Q_i\end{bmatrix} \tag{11}$$

where A_i and B_i represent the coefficient matrixes.

To again avoid excessive complexity, line impedances of the two converters are assumed equal, which together with the load impedance, are expressed as $Z = r + jX$ and $Z_L = R_L + jX_L$, respectively. The output current expressions of the converters can thus be expressed as:

$$[\Delta I] = [Y][\Delta V] \tag{12}$$

with $$[\Delta I] = \begin{bmatrix}\Delta I_{d1} & \Delta I_{q1} & \Delta I_{d2} & \Delta I_{q2}\end{bmatrix}^T$$

$$[\Delta V] = \begin{bmatrix}\Delta V_{d1} & \Delta V_{q1} & \Delta V_{d2} & \Delta V_{q2}\end{bmatrix}^T$$

where [Y] is the nodal admittance matrix, and I_{di} and I_{qi} are real and imaginary components of each converter output current.

Active and reactive powers of each converter can then be computed using (13), which upon perturbed, leads to (14).

$$\begin{cases}P_i = V_{di}I_{di} + V_{qi}I_{qi}\\ Q_i = V_{qi}I_{di} - V_{di}I_{qi}\end{cases} \tag{13}$$

$$[\Delta S] = [I][\Delta V] + [V][\Delta I] \tag{14}$$

where $[\Delta S] = \begin{bmatrix}\Delta P_1 & \Delta Q_1 & \Delta P_2 & \Delta Q_2\end{bmatrix}^T$.

The state equation of the whole system with two converters can hence be represented as:

$$[\Delta\dot{X}] = \left\{\begin{bmatrix}A_1 & 0\\ 0 & A_2\end{bmatrix} + \begin{bmatrix}B_1 & 0\\ 0 & B_2\end{bmatrix}\left([I] + [V][Y]\right)[k]\right\}[\Delta X] \tag{15}$$

where

$$[\Delta X] = \begin{bmatrix}\Delta V_{DC1} & \Delta f_1 & \Delta V_{d1} & \Delta V_{q1} & \Delta V_{DC2} & \Delta f_2 & \Delta V_{d2} & \Delta V_{q2}\end{bmatrix}^{\mathrm{T}},$$

$$[k] = \begin{bmatrix}0&0&1&0&0&0&0&0\\ 0&0&0&1&0&0&0&0\\ 0&0&0&0&0&0&1&0\\ 0&0&0&0&0&0&0&1\end{bmatrix}.$$

From (15), the state space matrix M for the whole system can eventually be extracted as:

$$M = \begin{bmatrix}A_1 & 0\\ 0 & A_2\end{bmatrix} + \begin{bmatrix}B_1 & 0\\ 0 & B_2\end{bmatrix}\left([I] + [V][Y]\right)[k]. \tag{16}$$

Using (16), root loci can be plotted for analyzing the system response with $\dot{V}_1 = \dot{V}_2 = 218 + j30$V, for the converters, Z_L = 50+j0.2Ω for the load, Z = 2+j0.1Ω for the distribution lines, and ω_f = 3.141 rad/s for the common cut-off frequency of the low-pass filters used for computing the average powers. With droop coefficients next set as k_p = 0.004, k_q = 0.001 and k_V changing from 0.05 to 0.5, Fig. 4 shows the first set of root loci plotted. The dominant poles λ_2 and λ_3 noted in the figure are

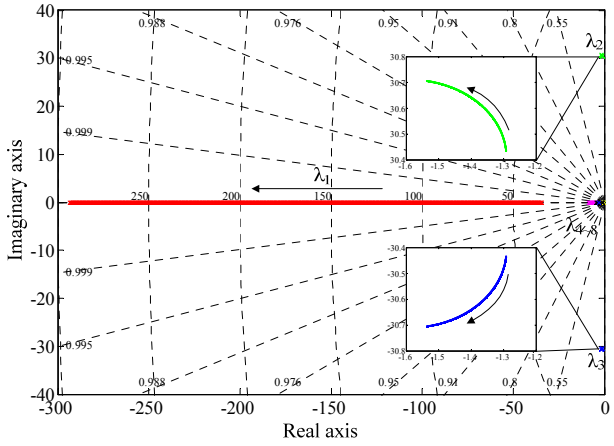

Fig. 4. Root locus diagram for $0.05 \le k_V \le 0.5$.

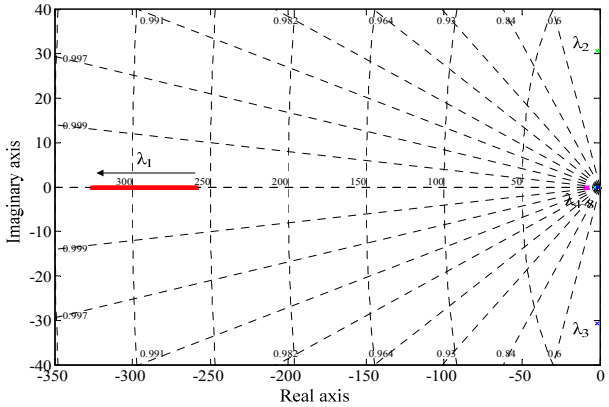

Fig. 5. Root locus diagram for $0.0001 \le k_p \le 0.1$ with improved droop scheme.

found to shift away from the imaginary axis, as k_V increases. The expectation is thus an improvement of system dynamics, while retaining stability since all poles are still in the left-half s-plane. Fig. 5 follows with another set of root loci obtained with k_q = 0.001, k_V = 0.4 and k_p varying from 0.0001 to 0.1. Only two poles λ_2 and λ_3 are again found to affect the system dynamics, since the other poles are far away from the imaginary axis. Despite that, the system is still stable.

Finally, Fig. 6 shows the last set of root loci, where the coefficient changed is k_q from 0.0001 to 0.1, while keeping the others constant at k_p = 0.004 and k_V =0.4. Since this combination of coefficients can lead to instability if not designed properly, it is plotted for both improved and traditional droop schemes for comparison. The traditional scheme referred to here is the scheme, which uses (3) and (4) for droop purposes. It is thus the same basic scheme used in [19] and many others found in the literature. Fig. 6(a) shows the root loci of the improved droop scheme, where it can be seen that dominant poles λ_2 and λ_3 shift closer to the imaginary axis, as k_q increases. The system response will therefore become more oscillatory, and eventually destabilize, as k_q rises above 0.0377 (λ_2 and λ_3 enter the right-half s-plane). In contrast, response of the traditional droop scheme is dominated by the single pole λ_3, which will move closer to the imaginary axis, as k_q increases. The system eventually becomes unstable, as k_q rises above

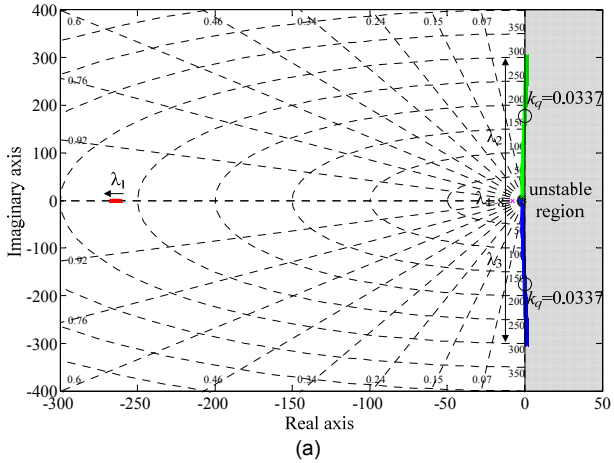

(a)

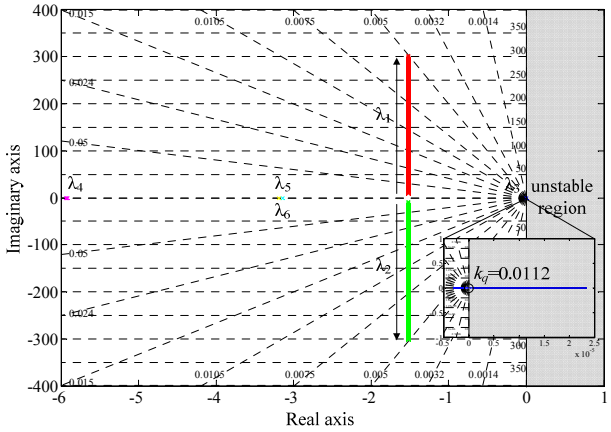

(b)

Fig. 6. Root locus diagram for $0.0001 \le k_q \le 0.1$ (a) improved droop scheme and (b) traditional droop scheme.

0.0112. The stable range of k_q of the improved droop scheme is thus wider than that of the traditional droop scheme. Besides this, stabilities of both droop schemes are not affected by normal variations of the converter and inverter output filters, since both schemes use only low-pass filtered or average power values.

IV. Grid-Connected Mode

For smoother operation, the same droop expressions should be used for the grid-connected mode [16], which also requires the PV inverter to output the maximum power P_{PVmax}. This maximum power can however be lower than the rated power P_0 in (3), depending on the operating conditions. The traditional droop expressions in (3) and (4) are therefore not directly applicable, and must hence be changed accordingly. One straightforward approach is given in (17):

$$V = \underbrace{V_0 - k_p(P - P_0)}_{} + \underbrace{(k_{pp} + \frac{k_{ip}}{s})(P_{PVmax} - P)}_{} \qquad (17)$$

where k_{pp} and k_{ip} are proportional and integral gains, respectively. The modification noted here is the second term of (17), which in effect, has added an offset ΔV_G ($-k_p P_0 \le \Delta V_G \le 0$) to the original droop line. The purpose is to make the system output the PV maximum power P_{PVmax}, rather than its rated

power P_0 ($P_{PVmax} \le P_0$). Moreover, unlike the islanded mode, power sharing is not the main concern in the grid-connected mode, which hence permits an integral term to be used in (17).

The same offset in (17) can also help to filter off influences from grid voltage and line impedance variations. For example, as shown in Fig. 2(b), the PV system is initially operating at point *c* with maximum PV power harnessed. The grid voltage *E* is subsequently assumed to change slightly, causing the power transfer curve from (1) to lower slightly. The new operating point of the inverter will then be at c_1, while the dc-dc converter remains at *c*. This condition is however unsustainable, since an imbalance in power exists between the dc-dc converter and inverter. The response from (17) will then be the lowering of droop line by ΔV_G, until the final operating point c_2 is reached. Finding ΔV_G from (17) is however not direct, since P_{PVmax} is unknown, if irradiation and temperature are not measured. Moreover, (17) does not permit the rear-end inverter, controlled by it, to regulate the dc-link voltage V_{DC}, which strictly, is necessary, since the front-end dc-dc converter is already tasked to track the PV maximum power point.

Expression (17) must hence be changed to (18), where its second term can be used for regulating the dc-link voltage by indirectly forcing the inverter output power to follow the PV maximum power.

$$V = \underbrace{V_0 - k_p(P - P_0)}_{} + \underbrace{(k_{pp} + \frac{k_{ip}}{s})(V_{DC} - V_{DCref})}_{} \quad (18)$$

Additionally, the gain k_{pp} in (18) should be chosen such that the maximum transient energy flowing through the dc-link capacitor does not cause its voltage to rise above its trip level. The gain k_{ip} should, on the other hand, be chosen to minimize the steady-state error. For the implemented system, they are respectively chosen as $k_{pp} = 0.0003$ and $k_{iq} = 0.005$, which are comparably low gains suitable for the slower outer droop control loop.

The same reasoning can be applied to (4), leading to the following modified *Q-f* expression:

$$f = \underbrace{f_0 + k_q(Q - Q_0)}_{} + \underbrace{(k_{pq} + \frac{k_{iq}}{s})(Q - Q_{ref})}_{} \quad (19)$$

where k_{pq} and k_{iq} are proportional and integral gains, respectively. Again, the first term of (19) is the usual droop expression, shifted vertically by the added second term to follow the demanded reference Q_{ref} (set to zero if unity power factor is preferred). Additionally, k_{pq} should be chosen to give a satisfactory dynamic response, while k_{iq} should be chosen to minimize the steady-state error. For the implemented PV system, these gains are set as $k_{pq} = 0.0001$ and $k_{iq} = 0.0004$ to give a sufficiently long response time needed for decoupling the slower outer droop power loop from the faster inner voltage and current tracking loops.

Fig. 7 shows the eventual grid-connected scheme implemented for the PV system. As usual, the boost converter is controlled by measuring V_{PV} and I_{PV} from the PV panel for tracking in the MPPT block. The inverter is however droop-controlled using almost the same control blocks as in Fig. 3 for the islanded mode, except with the improved droop expressions in (18) and (19) used instead. In addition, a harmonic detection block based on instantaneous power theory [35] has been used for extracting harmonic voltage v_h from the inverter terminal voltage v_{ac}. The voltage reference for tracking is then obtained by summing v_f and v_h, where v_f is the fundamental voltage reference produced by the droop controller. Voltage v_h is therefore not compensated, which according to (20), will result in a smaller grid current distortion i_h, caused by the grid voltage harmonics v_{Gh}.

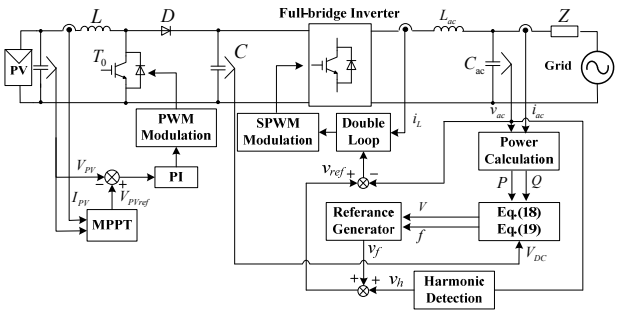

Fig. 7. Control scheme for two-stage PV system in grid-connected mode (transformer used in practice and experiment not shown for conciseness).

$$|i_h| = \left|\frac{v_h - v_{Gh}}{Z}\right| \le \left.\frac{|v_{Gh}|}{Z}\right|_{v_h \text{ forced to zero}} \quad (20)$$

The grid-connected scheme in Fig. 7 will hence function well, even though at times, it may encounter problems caused by large delivered PV power. More specifically, the large delivered PV power may cause the inverter output voltage v_{ac} to rise higher than threshold permitted by the local loads. When that happens, the front dc-dc boost converter should stop its upward stepping to the maximum power point. Instead, the curtailed power value should be used or the gradual stepping down of power should be activated until v_{ac} is brought below the permitted threshold.

V. Seamless Transfer

Comparing (6) and (4) for the islanded mode with (18) and (19) for the grid-connected mode, the generalized droop expressions for both modes can be comprehended, as follows:

$$V = V_0 - k_p(P - P_0) + (K_{PP} + \frac{K_{IP}}{s})(V_{DC} - V_{DCref})$$
$$K_{PP} = \begin{cases} k_{pp}, & grid-connected\ mode \\ k_V, & islanded\ mode \end{cases}$$
$$K_{IP} = \begin{cases} k_{ip}, & grid-connected\ mode \\ 0, & islanded\ mode \end{cases} \quad (21)$$

$$f = f_0 + k_q(Q - Q_0) + (K_{PQ} + \frac{K_{IQ}}{s})(Q - Q_{ref})$$
$$K_{PQ} = \begin{cases} k_{pq}, & grid-connected\ mode \\ 0, & islanded\ mode \end{cases}$$
$$K_{IQ} = \begin{cases} k_{iq}, & grid-connected\ mode \\ 0, & islanded\ mode \end{cases} \quad (22)$$

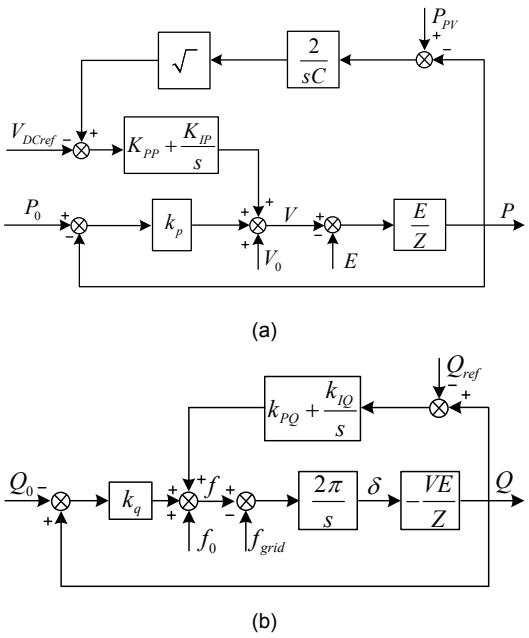

Fig. 8. Block diagrams illustrating improved (a) *P*-*V* and (b) *Q*-*f* droop control.

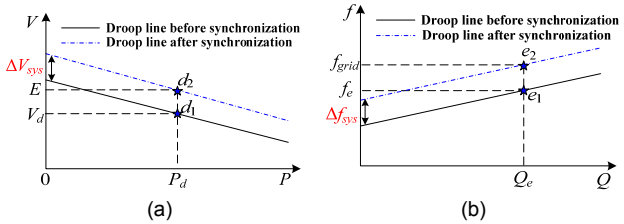

Fig. 9. Droop lines for illustrating (a) grid voltage and (b) grid frequency synchronizations.

Together with (1) and (2), block diagrams representing (21) and (22) can subsequently be drawn, as shown in Fig. 8(a) and (b). The same droop expressions in (21) and (22) can therefore be used for both modes with seamless transfer between them expected, since there are no major changes or swopping of control schemes. The boost converter will however experience changes from MPPT to dc-link voltage control, and vice versa. These changes are however decoupled by the dc-link capacitor, and will hence not disturb the grid significantly.

In addition, seamless transfer from the islanded to grid-connected mode requires synchronization with the grid, before static switch between the PV system and grid can be closed. The necessary synchronization can be explained with Fig. 9. Before synchronization, Fig. 9(a) shows the inverter operating at point d_1 with output voltage V_d and output power P_d generated for the local load. After initiating synchronization, P_d must be held constant to continuously meet the local load demand, while lifting the inverter voltage from V_d to the grid voltage E. Such lifting can again be realized by adding an autonomously generated vertical offset, expressed as follows.

$$\Delta V_{sys} = (k_{pV} + \frac{k_{iV}}{s})(E - V) \tag{23}$$

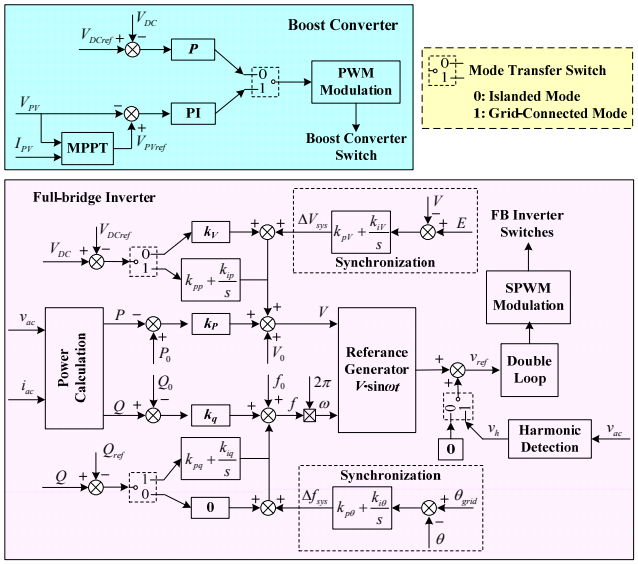

Fig. 10. Overview of improved droop scheme.

where k_{pV} and k_{iV} are proportional and integral gains of the voltage synchronizer.

The same applies to Fig. 9(b), where the initial reactive power Q_e must be maintained, while lifting the inverter frequency from f_e to the grid frequency f_{grid}. Lifting the frequency alone is however not sufficient, since the phase of the inverter θ may not be equal to that of the grid θ_{grid}. It is therefore important for the inverter to track the phase of the grid using (24), which upon achieved, will indirectly force the inverter to have the same frequency as the grid.

$$\Delta f_{sys} = (k_{p\theta} + \frac{k_{i\theta}}{s})(\theta_{grid} - \theta) \tag{24}$$

where $k_{p\theta}$ and $k_{i\theta}$ are proportional and integral gains of the phase synchronizer. These parameters and those in (23) are chosen as $k_{p\theta} = 10$, $k_{i\theta} = 20$, $k_{pV} = 3$ and $k_{iV} = 5$ to give a response time of around 0.2s for both synchronizers.

Expressions (23) and (24) are however not explicitly added to (21) and (22), since they are needed only during the short islanded to grid-connected transition. Instead, they are summarized with the other droop and offset expressions in Fig. 10. The necessary transfer procedures are also comprehended, as follows.

Grid-connected to islanded mode

- Detection of disconnection command.
- MPPT to dc-link voltage control for the boost converter.
- Same improved droop control for the inverter, but with parameters changed appropriately (see (21) and (22)).

Islanded to grid-connected mode

- Detection of connection command.
- Activation of synchronizers in (23) and (24).
- Closing of static switch after synchronization.
- Deactivation of synchronizers.
- DC-link voltage to MPPT control for the boost converter.
- Same droop control for the inverter, but with parameters changed appropriately (see (21) and (22)).

TABLE I
PARAMETERS OF TESTED SYSTEM

Parameters	Values
Panel voltage variation (V_{PV})	190V-300V
Grid voltage (E)	220V(rms)
Grid frequency (f_{grid})	50Hz
DC-link voltage (V_{DC})	400V
DC-link voltage capacitance (C)	940μF
Boost inductance (L)	4mH
Output filter inductance (L_{ac})	5mH
Output filter capacitance (C_{ac})	10μF
Inverter switching frequency (f_s)	10kHz
Impedance of transmission line (Z)	2Ω, 0.8μH

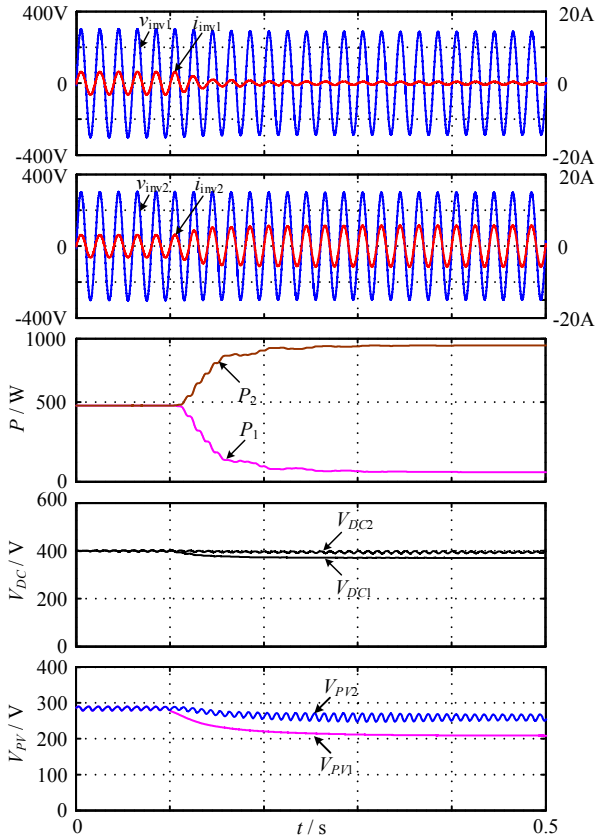

Fig. 11. Simulated results of two paralleled PV inverters using improved droop schemes.

VI. SIMULATION RESULTS

Two similarly rated PV systems, tied to a LV distribution network, have been simulated in Matlab/Simulink using parameters listed in Table I for each system. Results obtained from them are described below.

A. Islanded Mode for Evaluation of Internal Power Changes

Fig. 11 shows the results of the two islanded PV systems when controlled by the improved droop scheme. Before 0.1s, the two systems are assumed to have the same maximum rating of 1kW. They should hence share the active load demand evenly with their respective dc-link voltages kept at 400V (nominal value read from Table I). After 0.1s, the maximum power of one system has been reduced from 1kW to 60W, while that of the others remains unchanged. The compromised system, being unable to provide sufficient active power, will then have its dc-link voltage pulled down. The drop causes the droop line of the compromised system to be shifted down, like in Fig. 2. The droop-demanded output active power of the compromised system is then lowered until it reaches 60W. In the meantime, the second uncompromised system supplies more active power to the loads, which strictly, is necessary before supply and demand can be balanced. The overall network is therefore stable with only slight droops observed with the dc-link and inverter output voltages, even though the PV terminal voltages may change more prominently.

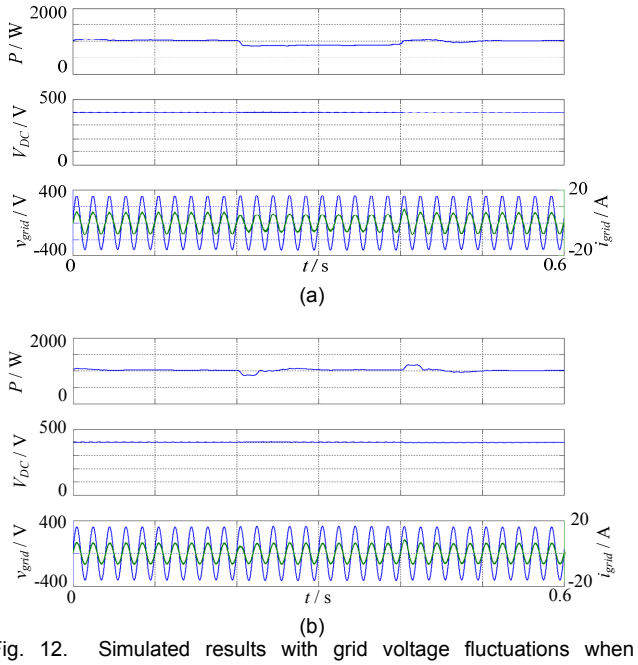

Fig. 12. Simulated results with grid voltage fluctuations when controlled with (a) traditional and (b) improved droop schemes.

B. Grid-Connected Mode for Evaluation of External Changes

As explained with (1) and (2), external disturbances are introduced through E and Z. Both parameters are prominently influenced by the grid. Results from the grid-connected mode are therefore chosen for demonstration (even though the same testing has also be performed in the islanded mode). As shown in Fig. 12(a), the grid voltages read are v_{grid} = 220V from 0 to 0.2s, 225V from 0.2s to 0.4s, and 220V from 0.4s to 0.6s. Throughout the three intervals, the maximum PV power has been set to P_{PVmax} = 1000W. However, with the traditional droop scheme, P_{PVmax} is not harnessed when the grid voltage increases in the second interval. The actual power generated is only 800W, delivered by a much smaller grid current i_{grid}. On the other hand, Fig. 12(b) shows the results obtained with the improved droop scheme when subject to the same changes. The harnessed power is now always 1000W, even though some slight variations can be observed at the instants of voltage changes. The proposed scheme is therefore more effective in terms of active power tracking.

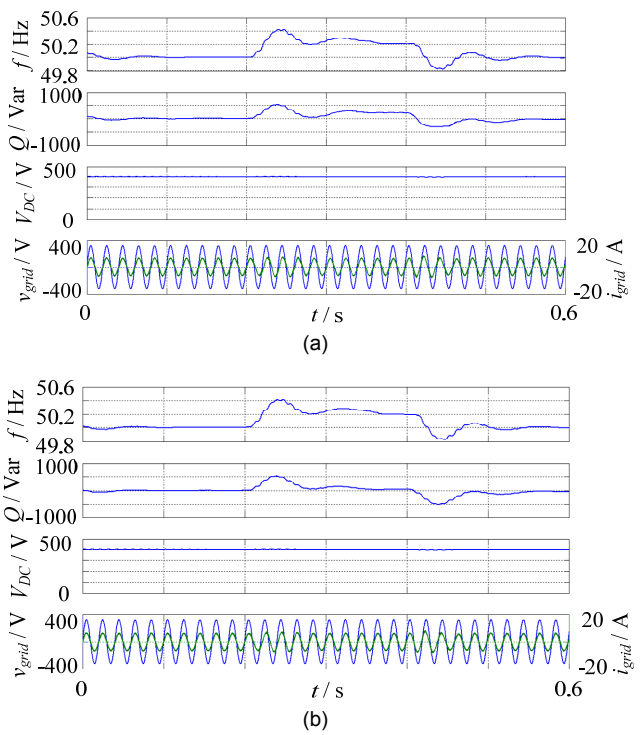

Fig. 13. Simulated results with grid frequency fluctuations when controlled with (a) traditional and (b) improved droop schemes.

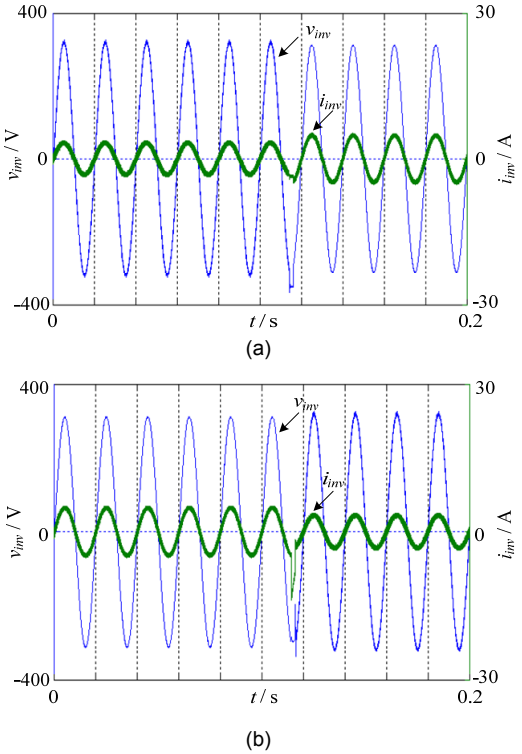

Fig. 14. Simulated results for showing (a) islanded to grid-connected transfer and (b) grid-connected to islanded transfer when controlled with traditional control scheme.

Fig. 13(a) and (b) next show the results obtained when the grid frequency increases from 50Hz to 50.2Hz during the interval from 0.2s to 0.4s. The former uses the traditional droop scheme, while the latter uses the improved droop scheme. The traditional droop scheme is obviously not able to regulate the reactive power at zero during the second interval (Q = 500VAr), which the improved scheme can achieve after some slight transient variations. The proposed scheme is thus less affected by grid frequency fluctuations, which surely, is encouraged.

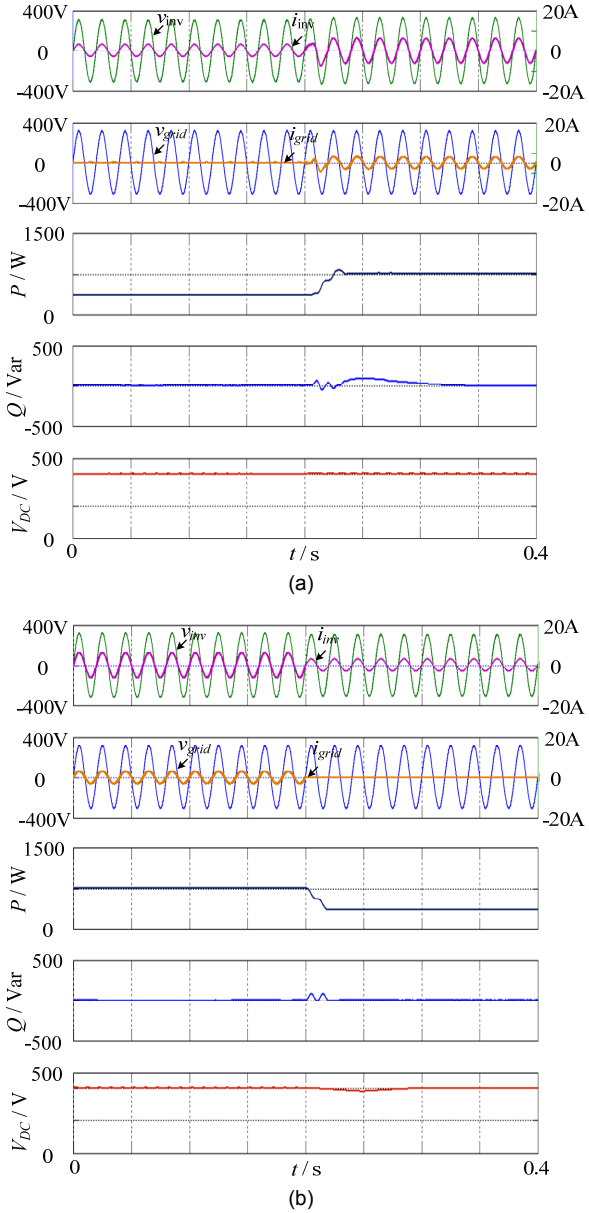

Fig. 15. Simulated results for showing (a) islanded to grid-connected transfer and (b) grid-connected to islanded transfer when controlled with improved droop scheme.

Some results are then included in Fig. 14(a) and (b) for showing how the traditional controlled system responds during mode transfers. Quite obviously, Fig. 14(a) shows the inverter voltage v_{inv} surging during the islanded to grid-connected transfer at 0.115s, while Fig. 14(b) shows the inverter current i_{inv} surging during the reverse grid-connected to islanded transfer. Such surging is however not seen in Fig. 15(a) and (b) at the transfer time of 0.2s. The transfers are hence seamless with the improved droop scheme.

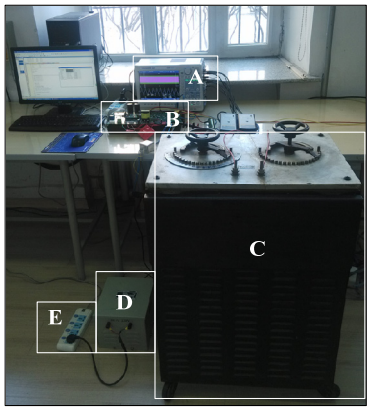

Fig. 16. Laboratory setup showing A -oscilloscope, B - PV inverter, C - load, D - line transformer, and E -point of common coupling.

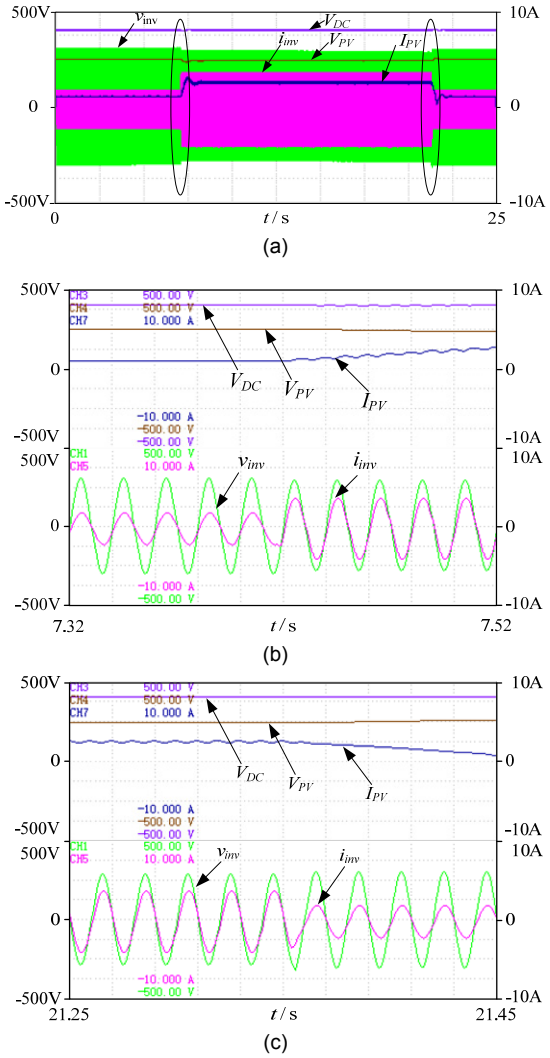

Fig. 17. Experimental results with load change. (a) Full view, (b) increasing load, and (c) decreasing load.

VII. Experimental Results

Experimental testing with a 1-kW PV system has been performed for proving the practicality of the proposed scheme.

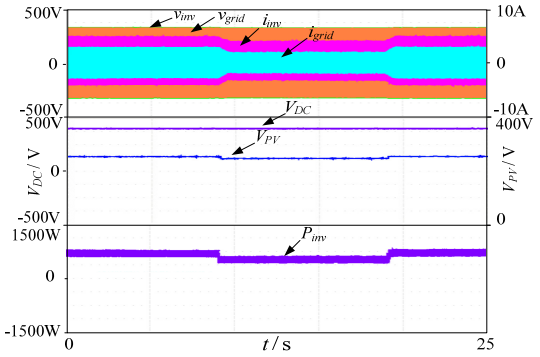

Fig. 18. Experimental results with maximum power fluctuations from PV panel when using improved droop scheme.

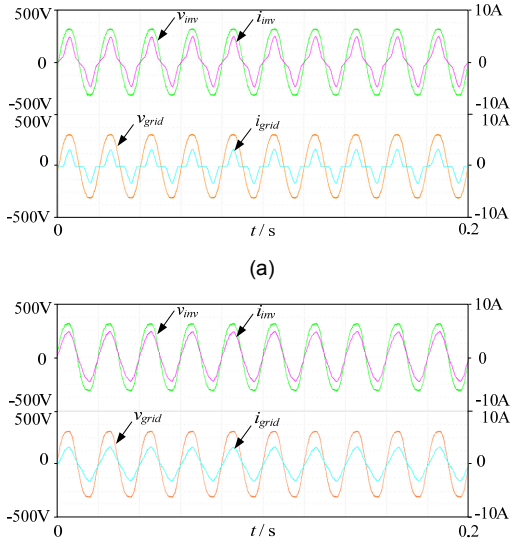

Fig. 19. Experimental results with grid voltage distortion. (a) without harmonic detection unit and (b) with harmonic detection unit.

The hardware setup is shown in Fig. 16, while its parameters are given in Table I. The dc source used is a *Chroma 62150H-600S* programmable supply, programmed to output typical PV characteristics, while the controller used is a 32-bit *STM32F103VBT6* microcontroller from *STMicroelectronics*. Results from the setup when first islanded are shown in Fig. 17 when the improved droop scheme is used, together with a load increase and then decrease. The load power is more specifically read as P_{Load} = 280W from 0 to 7.42s, 560W from 7.42s to 21.35s, and 280W from 21.35s to 25s. These powers are supplied by the PV source, whose terminal voltage will hence change from V_{PV} = 250V to 240V, and then back to 250V. Despite the changes, the results show that the PV inverter operates as intended with its dc-link voltage V_{DC} kept at the nominal of 400V, since no drop in PV capacity has been introduced yet.

Fig. 18 shows power fluctuations from the PV simulator, whose values have been read as P_{PVmax} = 700W from 0 to 9s, 500W from 9s to 19s, and 700W from 19s to 25s. These power changes, in turn, cause the panel voltage to change from V_{PV} = 246V to 240V and then back to 246V. Regardless of that, the

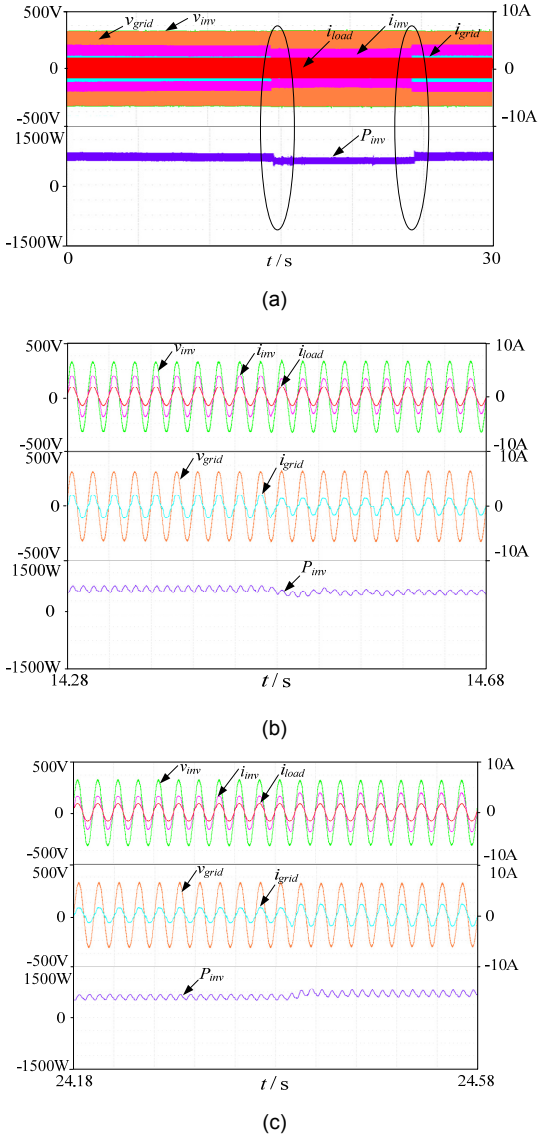

Fig. 20. Experimental results with grid voltage fluctuations when using traditional droop scheme. (a) Full view, (b) zoomed-in view of first transition, and (c) zoomed-in view of second transition.

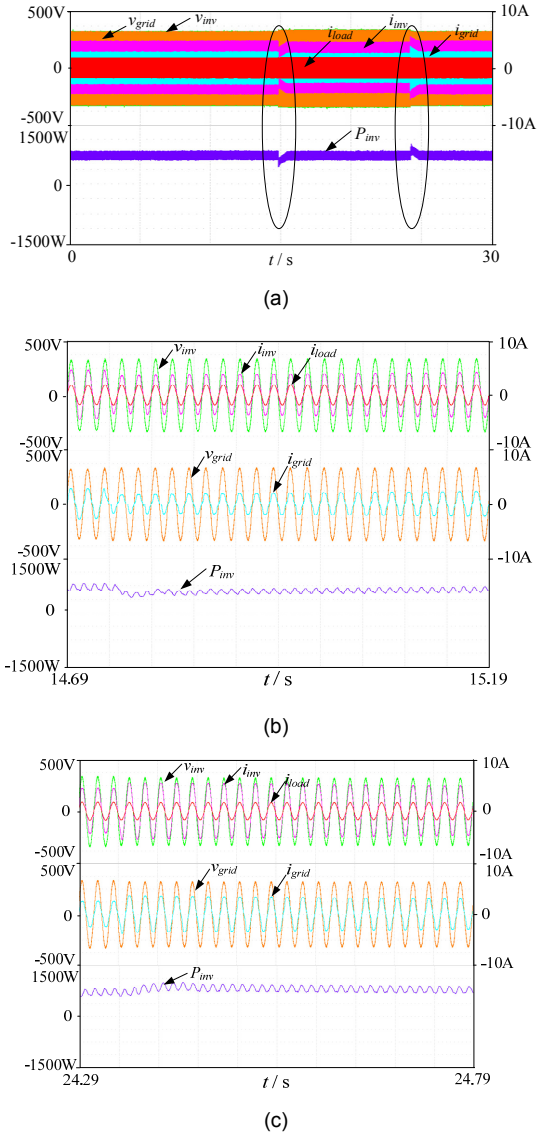

Fig. 21. Experimental results with grid voltage fluctuations when using improved droop scheme. (a) Full view, (b) zoomed-in view of first transition, and (c) zoomed-in view of second transition.

dc-link voltage is well-regulated at 400V by the improved droop scheme, while harnessing P_{PVmax} during the three intervals.

Fig. 19(a) next shows the results without the harmonic detection block in Fig. 7 for filtering out the grid voltage distortion. The observed inverter current and grid current are obviously distorted, as anticipated. These current distortions are however not seen in Fig. 19(b) when the harmonic detection block in Fig. 7 is enabled.

Fig. 20 then shows the results obtained with grid voltage v_{grid} fluctuations when controlled by the traditional droop scheme from (3) and (4) (v_{grid} = 220V from 0 to 14.48s, 225V from 14.48s to 24.38s, and 220V from 24.38s to 30s). As observed, maximum PV power of P_{PVmax} = 700W is only generated in the first and third intervals. Power generated in the second interval is only 560W because of the higher v_{grid}. Grid voltage fluctuations will therefore affect the maximum power harnessing ability of the system when controlled by the traditional droop scheme.

For comparison, Fig. 21 repeats the experiment with grid voltage fluctuations when controlled by the improved droop scheme from (21) and (22) (v_{grid} = 220V from 0 to 14.74s, 230V from 14.74s to 24.34s, and 220V from 24.34s to 30s). At the instant of grid voltage increase, the inverter power in Fig. 21(b) is noted to drop to 520W, before gradually returning to the maximum PV power of P_{PVmax} = 700W. In contrast, the decrease of grid voltage in Fig. 21(c) has caused the inverter power to increase to 880W, before returning to 700W. The extra power of 180W at the transition is supplied by the dc-link capacitor since the maximum PV power is only 700W. The proposed scheme is thus able to harness maximum active power even when subjected to grid voltage variations.

Instead of grid voltage, Fig. 22 shows the results obtained with the traditional droop scheme when subjected to grid

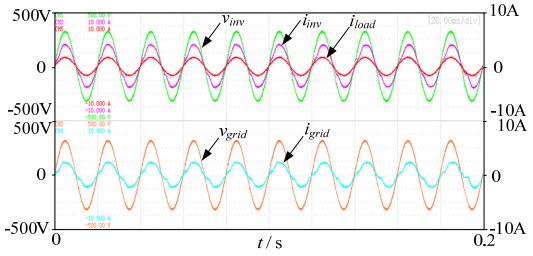

(a)

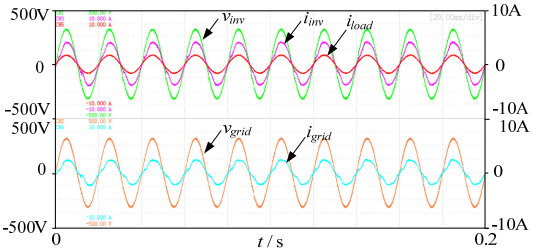

(b)

Fig. 22. Experimental results with grid frequency fluctuations when using traditional droop scheme. Grid frequency (a) increasing and (b) decreasing.

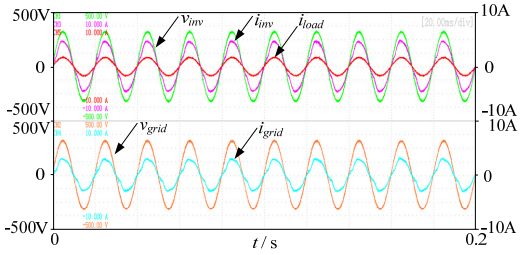

(a)

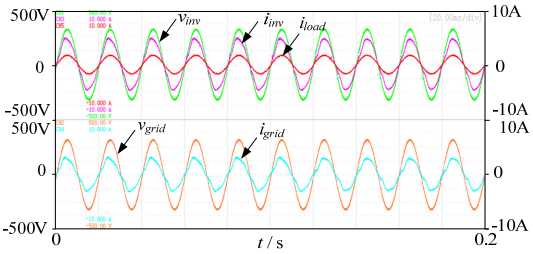

(b)

Fig. 23. Experimental results with grid frequency fluctuations when using improved droop scheme. Grid frequency (a) increasing and (b) decreasing.

frequency fluctuations. As seen from Fig. 22(a), the increase of grid frequency from 50Hz to 50.1Hz has caused the grid current to gradually lag behind the grid voltage. The output reactive power from the inverter is thus non-zero. It only returns to zero in Fig. 22(b) after the grid frequency returns from 50.1Hz to 50Hz. The same grid frequency testing has been repeated in Fig. 23, where Fig. 23(a) shows the grid current lagging initially, before returning to its in-phase position when the grid frequency increases from 50Hz to 50.1Hz. Fig. 23(b) also shows the gradual returning of reactive power to zero when the grid frequency decreases from 50.1Hz to 50 Hz. The improved

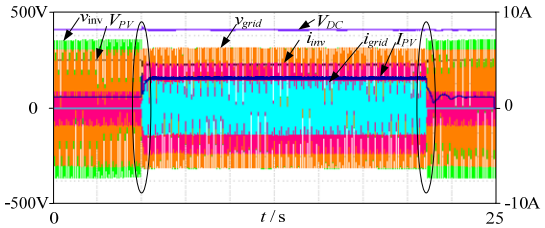

(a)

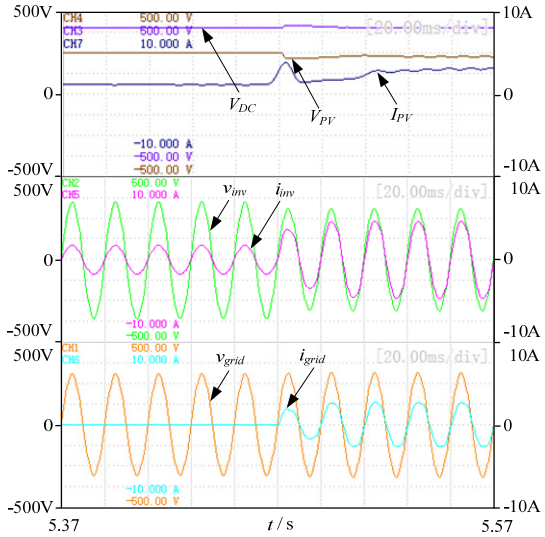

(b)

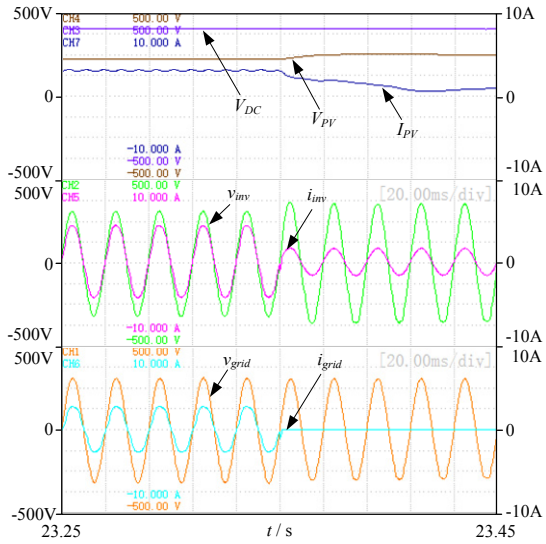

(c)

Fig. 24. Experimental results showing mode transfers with the improved droop scheme. (a) Full view, (b) islanded to grid-connected transfer, and (c) grid-connected to islanded transfer.

droop scheme is thus able to track reactive power more accurately even when the grid frequency fluctuates.

Last but not least, Fig. 24 shows the experimental transfer from islanded to grid-connected mode at 5.47s and the reverse transfer from grid-connected to islanded mode at 23.35s. Their zoomed-in views are provided in Fig. 24(b) and (c), respectively. As seen from Fig. 24(b), the inverter with its

stable dc-link voltage is found to supply only 280W to the local load, before the transfer. The grid current read is also at zero initially. The output voltage of the inverter is then activated to track the grid voltage, which upon synchronized, permits the static switch to close to start the transfer. After the transfer, the inverter and grid currents are noted to increase since the full maximum PV power is harnessed with 280W flowing to the load and 420W flowing to the grid (total = P_{PVmax} =700W). During this time, the PV terminal voltage is also observed to drop from 250V to 225V, caused by its larger amount of power generated.

Based on the same reasons, the reverse transfer in Fig. 24(c) also correctly shows the inverter current decreasing and grid current falling to zero after entering the islanded mode. The inverter now generates only 280W for the local load even though the maximum power available is 700W. Overall, the two transfers have been seamless with no disturbing transients observed. This is partly due to the synchronizers used, and partly due to the common improved droop structure used for both operating modes.

VIII. Conclusion

An improved droop scheme has been proposed in the paper for a PV system connected to a resistive LV distribution network. The approach is developed for a two-stage PV system, permitting it to transfer seamlessly between the islanded and grid-connected modes, after ensuring proper synchronization. It also allows the PV system to generate maximum active power, while remain not affected by power fluctuations, and other grid voltage and frequency disturbances when in the grid-connected mode. Such immunity is realized by dynamically shifting the droop lines in both grid-connected and islanded modes. Simulation and experimental results have verified the performances of the proposed method.

References

[1] S. A. Arefifar, and Y. A. –R. I. Mohamed, "Probabilistic optimal reactive power planning in distribution systems with renewable resources in grid-connected and islanded modes," *IEEE Trans. Ind. Electron*., vol. 61, no. 11, pp. 5830–5839, Nov. 2014.

[2] M. Pereira, D. Limon, D. Munoz de la Pena, L. Valverde, and T. Alamo, "Periodic economic control of a nonisolated microgrid," *IEEE Trans. Ind. Electron*., vol. 62, no. 8, pp. 5247–5255, Aug. 2015.

[3] Q. Shafiee, C. Stefanovic, T. Dragicevic, P. Popovski, J. C. Vasquez, and J. M. Guerrero, "Robust networked control scheme for distributed secondary control of islanded microgrids," *IEEE Trans. Ind. Electron*., vol. 61, no. 10, pp. 5363–5374, Oct. 2014.

[4] Q. N. Trinh, and H. H. Lee, "An enhanced grid current compensator for grid-connected distributed generation under nonlinear loads and grid voltage distortions," *IEEE Trans. Ind. Electron*., vol. 61, no. 12, pp. 6528–6537, Dec. 2014.

[5] S. D. Reddy, M. P. Selvan, and S. Moorthi, "Design, operation, and control of S3 inverter for single-phase microgrid applications," *IEEE Trans. Ind. Electron*., vol. 62, no. 9, pp. 5569–5577, Sep. 2015.

[6] L. Hadjidemetriou, E. Kyriakides, and F. Blaabjerg, "A robust synchronization to enhance the power quality of renewable energy systems," *IEEE Trans. Ind. Electron*., vol. 62, no. 8, pp. 4858–4868, Aug. 2015.

[7] R. A. Mastromauro, M. Liserre, T. Kerekes, and A. Dell'Aquila, "A single-phase voltage-controlled grid-connected photovoltaic system with power quality conditioner functionality," *IEEE Trans. Ind. Electron*., vol. 56, no. 11, pp. 4436–4444, Nov. 2009.

[8] H. Kim, T. Yu, and S. Choi, "Indirect current control algorithm for utility interactive inverters in distributed generation systems," *IEEE Trans. Power Electron*., vol. 23, no. 3, pp. 1342–1347, May 2008.

[9] J. Kwon, S. Yoon, and S. Choi, "Indirect current control for seamless transfer of three-phase utility interactive inverters," *IEEE Trans. Power Electron*., vol. 27, no. 2, pp. 773–781, Feb. 2012.

[10] S. Yoon, H. Oh, and S. Choi, "Controller design and implementation of Indirect current control based utility-interactive inverter system," *IEEE Trans. Power Electron*., vol. 28, no. 1, pp. 26–30, Jan. 2013.

[11] Z. Liu and J. J. Liu, "Indirect current control based seamless transfer of three-phase inverter in distributed generation," *IEEE Trans. Power Electron*., vol. 29, no. 7, pp. 3368–3383, Jul. 2014.

[12] A. Micallef, M. Apap, C. Spiteri-Staines, J. M. Guerrero, and J. C. Vasquez, "Reactive power sharing and voltage harmonic distortion compensation of droop controlled single phase islanded microgrids," *IEEE Trans. Smart Grid*, vol. 5, no. 3, pp. 1149–1158, Nov. 2014.

[13] I. U. Nutkani, P. C. Loh, P. Wang, and F. Blaabjerg, "Autonomous droop scheme with reduced generation cost," *IEEE Trans. Ind. Electron*., vol. 61, no. 12, pp. 6803–6811, Dec. 2014.

[14] J. W. He, Y. W. Li, and F. Blaabjerg, "An Enhanced islanding microgrid reactive power, imbalance power, and harmonic power sharing scheme," *IEEE Trans. Power Electron*., vol. 30, no. 6, pp. 3389–3401, Jun. 2015.

[15] A. Kahrobaeian and Y. A. -R. I. Mohamed, "Analysis and mitigation of low-frequency instabilities in autonomous medium-voltage converter-based microgrids with dynamic loads," *IEEE Trans. Ind. Electron*., vol. 61, no. 4, pp. 1643–1658, Apr. 2014.

[16] Y. W. Li, D. M. Vilathgamuwa, and P. C. Loh, "Design, analysis, and real-time testing of a controller for multibus microgrid system," *IEEE Trans. Power Electron*., vol. 19, no. 5, pp. 1195–1204, Sep. 2004.

[17] J. C. Vasquez, J. M. Guerrero, M. Savaghebi, J. Eloy-Garcia, and R. Teodorescu, "Modeling, analysis, and design of stationary reference frame droop controlled parallel three-phase voltage source inverters," *IEEE Trans. Ind. Electron*., vol. 60, no. 4, pp. 1271–1280, Apr. 2013.

[18] M. Savaghebi, J. M. Guerrero, A. Jalilian, and J. C. Vasquez, "Mitigation of voltage and current harmonics in grid-connected microgrids," in Proc. *IEEE ISIE*, May 2012,pp. 1610–1615.

[19] W. Du, Q. R. Jiang, M. J. Erickson, and R. H. Lasseter, "Voltage-source control of PV inverter in a CERTS microgrid," *IEEE Trans. Power Del*., vol. 29, no. 4, pp. 1726–1734, Aug. 2014.

[20] A. Elrayyah, Y. Sozer, and M. Elbuluk, "Microgrid-connected PV-based sources: a novel autonomous control method for maintaining maximum power," *IEEE Ind. Applicat. Mag*., vol. 21, no. 2, pp. 19–29, Mar./Apr. 2015.

[21] T. S. Hwang, and S. Y. Park, "A seamless control strategy of a distributed generation inverter for the critical load safety under strict grid disturbances," *IEEE Trans. Power Electron*., vol. 28, no. 10, pp. 4780–4790, Oct. 2013.

[22] T. V. Tran, T. W. Chun, H. H. Lee, H. G. Kim, and E. C. Nho, "Pll-based seamless transfer control between grid-connected and islanding modes in grid-connected inverters," *IEEE Trans. Power Electron*., vol. 29, no. 10, pp. 5218–5228, Oct. 2014.

[23] R. –R. Wai, C. –Y. Lin, and Y. –C. Huang, "Design of high-perfromance stand-alone and grid-connected inverter for distributed generation applications," *IEEE Trans. Ind. Electron*., vol. 60, no. 4, pp. 1542–1555, Apr. 2013.

[24] X. H. Wang, C. J. Zhang, X. Li, and Z. N. Guo, "Weighted control research on seamless transfer for dual-mode three phase inverter in micro-grid," in *Int. Conf. Electr. Mach. Syst., ICEMS*, Beijing, China, 2011, pp. 1-5.

[25] D. Velaso DE La Fuente, C. L. T. Rodriguez, G. Garcero, E. Figueres, and R. O. Gonzalez, "Photovoltaic power system with battery backup with grid-connected and islanded operation capabilities," *IEEE Trans. Ind. Electron*., vol. 60, no. 4, pp. 1571–1582, Apr. 2013.

[26] C. Trujillo Rodriguez, D. Velasco De La Fuente, G. Garcera, E. Figueres, and J. A. Guacaneme Moreno, "Reconfigurable control scheme for a PV microinverter working in both grid-connected and island modes," *IEEE Trans. Ind. Electron*., vol. 60, no. 4, pp. 1582–1595, Apr. 2013.

[27] J. W. He, Y. W. Li, and M. S. Munir, "A flexible harmonic control approach through voltage-controlled DG-grid interfacing converters," *IEEE Trans. Ind. Electron*., vol. 59, no. 1, pp. 444–455, Jan. 2012.

[28] M. A. Abusara, J. M. Guerrero, and S. M. Sharkh, "Line-interactive UPS for microgrids," *IEEE Trans. Ind. Electron*., vol. 61, no. 3, pp. 1292–1300, Mar. 2014.

[29] C. I. Chen, "A phasor estimator for synchronization between power grid and distributed generation system," *IEEE Trans. Ind. Electron.*, vol. 60 no. 8, pp. 3248–3255, Aug. 2013.
[30] M. A. Zamani, T. S. Tarlochan, and A. Yazdani, "Investigations into the control and protection of an existing distribution network to operate as a microgrid: a case study," *IEEE Trans. Ind. Electron.*, vol. 61 no. 4, pp. 1904–1915, Apr. 2014.
[31] R. J. Wai, C. Y. Lin, Y. C. Huang, and Y. R. Chang, "Design of high-performance stand-alone and grid-connected inverter for distributed generation applications," *IEEE Trans. Ind. Electron.*, vol. 60 no. 4, pp. 1542–1555, Apr. 2013.
[32] C. T. Lee, R. P. Jiang, and P. T. Cheng, "A grid synchronization method for droop-controlled distributed energy resource converters," *IEEE Trans. Ind. Appl.*, vol. 49 no. 2, pp. 954–962, Mar/Apr. 2013.
[33] T. L. Vandoorn, B. Meersman, J. D. M. De Kooning, and L. Vandevelde, "Analogy between conventional grid control and island microgrid control based on a global DC-link voltage droop," *IEEE Trans. Power Delt.*, vol. 27, no. 3, pp. 1405–1414, Jul. 2012.
[34] H. Han, Y. Liu, M. Su, and J. M. Gueerrero, "An improved droop control strategy for reactive power sharing in islanded microgrid," *IEEE Trans. Power Electron.*, vol. 30, no. 6, pp. 3133–3141, Jun. 2015.
[35] Y. Q. Wang, L. Y. Yao, J. F. Peng, Y. L. Wang, and X. H. Mao "Analysis of Harmonic current suppression and reactive power compensation on 125 MVA motor generator," *IEEE Trans. Plasma Sci.*, vol. 40, no. 3, pp. 705–709, Mar.2012.

Hongpeng Liu (M'13) received his B.S. degree in Electrical Engineering from Harbin University of Science and Technology, Harbin, China, in 2000, and his M.S. and Ph.D. degrees in Electrical Engineering from Harbin Institute of Technology, Harbin, China, in 2006 and 2011, respectively. In 2011, he joined Harbin Institute of Technology as an Assistant Professor in the Department of Electrical Engineering. His current research interests include photovoltaic generation, Micro-grid, and PWM converter/inverter systems.

Poh Chiang Loh received his B. Eng (Hons) and M.Eng from the National University of Singapore in 1998 and 2000 respectively, and his Ph.D from Monash University, Australia, in 2002, all in electrical engineering. His interests are in power converters and their grid applications.

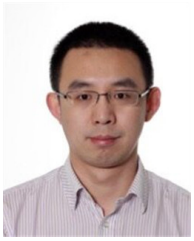

Xiongfei Wang (S'10-M'13) received the B.S. degree from Yanshan University, Qinhuangdao, China, in 2006, the M.S. degree from Harbin Institute of Technology, Harbin, China, in 2008, both in electrical engineering, and the Ph.D. degree from Aalborg University, Aalborg, Denmark, in 2013. Since 2009, he has been with the Aalborg University, Aalborg, Denmark, where he is currently an Assistant Professor in the Department of Energy Technology. His research interests include modeling and control of grid-connected converters, harmonics analysis and control, passive and active filters, stability of power electronic based power systems.

He received an IEEE Power Electronics Transactions Prize Paper award in 2014. He serves as the Associate Editor of IEEE Transactions on Industry Applications and the Guest Associate Editor of IEEE Journal of Emerging and Selected Topics in Power Electronics Special Issue on Distributed Generation.

Yongheng Yang (S'12 - M'15) received the B.Eng. degree from Northwestern Polytechnical University, Xian, China, in 2009, and the Ph.D. degree from Aalborg University, Aalborg, Denmark, in 2014.

He was a Post-Graduate with Southeast University, Nanjing, China, from 2009 to 2011. In 2013, he was a Visiting Scholar with the Department of Electrical and Computer Engineering, Texas A&M University, College Station, USA. Since 2014, he has been with the Department of Energy Technology, Aalborg University, where he is currently an Assistant Professor. His research interests are focused on grid integration of renewable energy systems, power converter design, analysis and control, harmonics identification and mitigation, and reliability in power electronics.

Dr. Yang is a Member of the IEEE Power Electronics Society Students and Young Professionals Committee, where he is responsible for the webinar series. He serves as a Guest Associate Editor of the IEEE Journal of Emerging and Selected Topics in Power Electronics special issue on Power Electronics for Energy Efficient Buildings. Dr. Yang has also been invited as a Guest Editor of Applied Sciences special issue on Advancing Grid-Connected Renewable Generation Systems. He is an active reviewer for relevant top-tier journals.

Wei Wang (M'13) received her B.S. degree in Automatic Test and Control from Harbin Institute of Technology, Harbin, China, in 1984, her M.S. degree in Electrical Engineering from Harbin Institute of Technology in 1990, and her Ph.D. degree in Mechanical Electronic Engineering from Harbin Institute of Technology in 2002. In 1984, she joined Harbin Institute of Technology, as an Assistant Professor in the Department of Electrical Engineering, where she was an Associate Professor from 1995 to 2003, and where she has been a Professor since 2003. She current research interests include regenerative energy converter techniques, micro-grid, soft-switching converters, and lighting electronic technology.

Dianguo Xu (M'97, SM'12) received the B.S. degree in Control Engineering from Harbin Engineering University, Harbin, China, in 1982, and the M.S. and Ph.D. degrees in Electrical Engineering from Harbin Institute of Technology (HIT), Harbin, China, in 1984 and 1989 respectively.

In 1984, he joined the Department of Electrical Engineering, HIT as an assistant professor. Since 1994, he has been a professor in the Department of Electrical Engineering, HIT. He was the Dean of School of Electrical Engineering and Automation, HIT from 2000 to 2010. He is now the assistant president of HIT. His research interests include renewable energy generation technology, power quality mitigation, sensorless vector controlled motor drives, high performance PMSM servo system. He published over 600 technical papers.

Dr. Xu is a senior member of IEEE, an Associate Editor for the IEEE Transactions on Industrial Electronics. He serves as Chairman of IEEE Harbin Section.